Supporting Information
Small Angle X-Ray Scattering as a Multifaceted Tool for Structural Characterization of Covalent Organic Frameworks

Renata A. Maia,[†] Leonardo S. A. Carneiro,[‡] Jhonny M. C. Cifuentes,[‡] Camilla D. Buarque,[‡] Pierre M. Esteves,[*,†] and Ana M. Percebom[*,‡]

†*Instituto de Química, Universidade Federal do Rio de Janeiro, Av. Athos da Silveira Ramos, 149, CT, Bl. A-622, Cid. Universitária, Ilha do Fundão, Rio de Janeiro, RJ, 21941-909, Brazil*

‡*Departament of Chemistry, Pontifical Catholic University of Rio de Janeiro, PUC-Rio, Rua Marquês de São Vicente, 225, Gávea, Rio de Janeiro, RJ, 22451-900, Brazil*

E-mail: pesteves@iq.ufrj.br; apercebom@puc-rio.br

Contents

1 Theory

1.1 Guinier's Approximation

Guinier's approximation[1] expresses the asymptotic behaviour for small values of q. In 1939, Guinier demonstrated (Equation 1) that for sufficiently small values of q there is a linear fit of ln[$I(q)$] versus q^2. Thus, affording the radius of gyration (R_g) of the scattering object and the scattered intensity at zero angle ($2\theta = 0°$) *I(0)*, from the slope and y-intercept, respectively.

$$I(q) = I(0) \exp \frac{-q^2 R_g^2}{3} \tag{1}$$

The parameter R_g is model-independent, meaning that it contains no information about the shape or the internal structure of the scattering object. It is the root-mean-square of the distances of all the electrons from their centre of gravity, thus corresponding to the radius of inertia in mechanics. However, if the scattering object structure could be assumed, R_g could be used to calculate its dimensions, assuming that R_g is the radius for the chosen geometrical shape.[2] Moreover, *I(0)* is related to the number of scattering objects and particle volume. Thus, it cannot be directly measured since it cannot be set apart from the incident radiation beam.

1.2 Porod's Law

Porod's law (Equation 2) expresses the asymptotic behaviour for high values of q. It was initially proposed that the small-angle scattering of an average smooth surface (*I(q)*) yields the well-known Debye-Porod q^{-4} power-law:[3]

$$I(q) = (\Delta\rho)^2 \cdot \frac{2\pi}{q^4} \cdot S \tag{2}$$

where $\Delta\rho$ is the contrast term and S is the specific surface of the scattering object.

However, most materials with fractal surfaces do not follow this decay. Because of that, this law has been extended[4] to accommodate rougher surfaces, in which a characteristic asymptotic power-law of $q^{-\alpha}$ is useful to determinate the fractal scale of the desired material with α values. The fractal scale is related to the statistic description of the scattering object properties, which can be expressed whether in mass fractal dimension or in surface fractal dimension parameters. Mass fractal dimension (D_m) is related to the packing of primary particles (sub-units with radius R_s) into larger aggregates with radius R_g (Figure S1). Meanwhile, the surface fractal dimension (D_s) does not consider explicitly primary particles as building blocks for the scattering object, due to the fact that its dimensions cannot be associated with the particles intern packing efficiency and it considers just the contribution of apparently dense objects for these aggregates.[5] Thus, $D_m = \alpha$ for the range of $1 < \alpha < 3$ and $D_s = 6 - \alpha$ for the range of $3 < \alpha < 4$. For a smooth boundary surface, $D_s = 2$, representing the Porod's law classical exponential of $\alpha = 4$. However, when a fractal scale is present, α assumes values smaller than 4.[6]

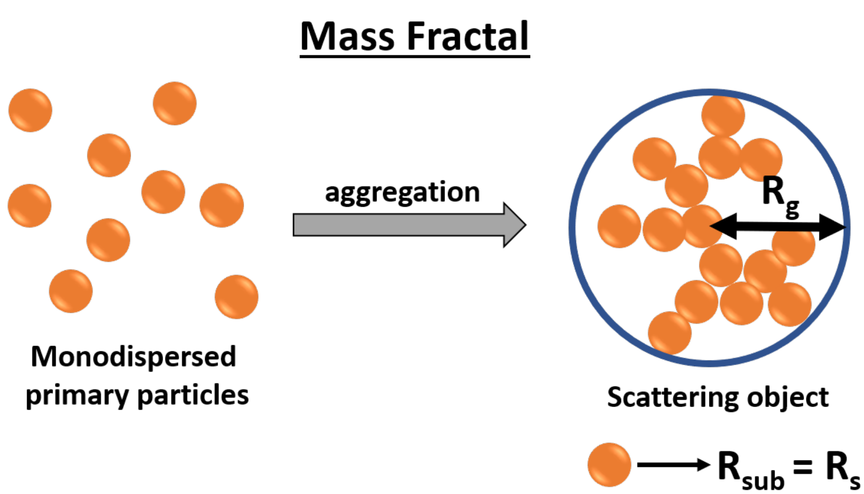

Figure S1: Mass fractal of the scattering object that originates from the aggregation of primary particles (sub-units)

2 Experimental Procedures and Characterizations

2.1 RIO-14

A pyrex pressure vessel (o.d. x i.d. = 2.5 x 1.6 cm^2 and length 10 cm, ChemGlass, mod. CG-1880-04) was charged with 1,3,4-triformylresorcinol (0.3882 g, 2 mmol) and tetrakis(4-aminophenyl)methane (1.14 g, 3 mmol). The top of the tube was closed with a rubber septum and the atmosphere was exchanged with argon. After that, 13.6 mL of dioxane, 1.2 mL of mesitylene and 4.6 mL of 6 M aqueous acetic acid were added. The tube was closed with a teflon cork and heated at 120 °C for 72 h, yielding a yellow solid at the bottom at the tube, which was isolated by filtration and washed with anhydrous dioxane and tetrahydrofuran (THF). The resulting powder was soaked in THF for three days to unclog the pores. After that, the material was filtered off and dried under vaccum, resulting in 2.645 g of the product.

2.2 $[HC\equiv C]_{0.17}$TPB-DMTP-COF

A pyrex pressure vessel (o.d. x i.d. = 2.5 x 1.6 cm^2 and length 10 cm, ChemGlass, mod. CG-1880-04) was charged with 1,3,5-Tris(4-aminophenyl)benzene (56.2 mg, 0.159 mmol), 2,5-dimethoxyterephthalaldehyde (31.0 mg, 0.159 mmol) and 2,5-bis(prop-2-yn-yloxy)terephthal-aldehyde (9.7 mg, 0.040 mmol). The top of the tube was closed with a rubber septum and the atmosphere was exchanged with argon. After that, a solution of *o*-DCB/n-BuOH (1:1 mL) and 0.2 mL of 6 M aqueous acetic acid was added. The tube was closed with a teflon cork and heated at 120 °C for 72 h, yielding a yellow solid, which was isolated by filtration and washed with anhydrous THF. The resulting powder was soaked in THF for three days to unclog the pores. Finally, the as-mentioned material was dried at 100°C in a vacuum oven for approximately 24 h, yielding a light yellow solid.

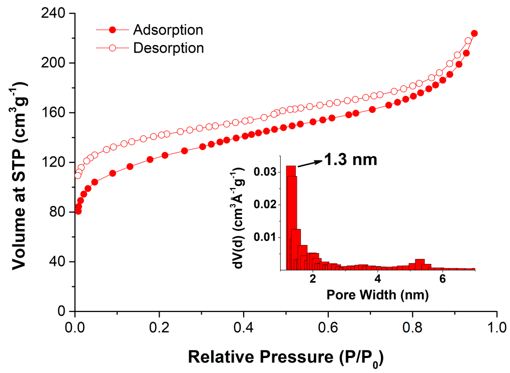

(a)

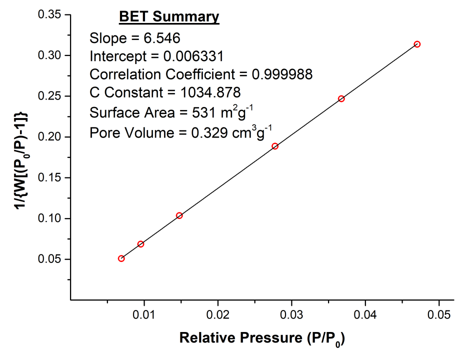

(b)

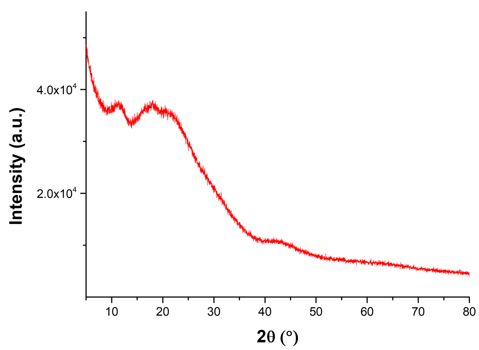

(c)

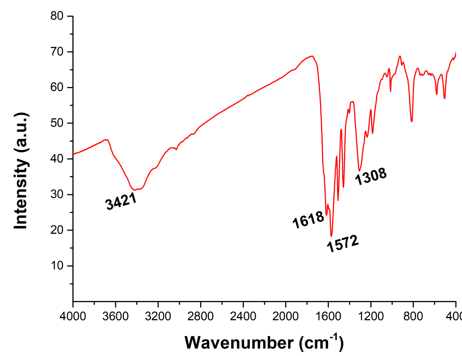

(d)

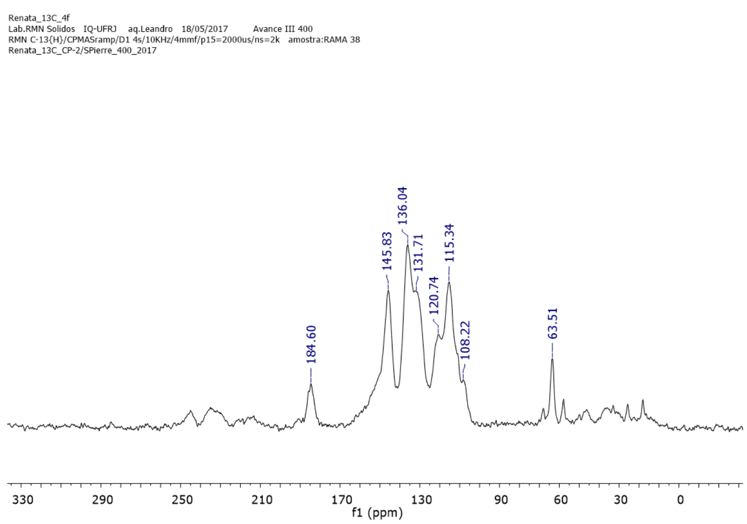

(e)

Figure S2: (a) Adsorption-desorption N_2 isotherm and pore size distribution using NLDFT equilibrium model for cylindrical pores. (b) Multi-point BET plot (c) PXRD, (d) FT-IR and (e) CP-MAS ^{13}C NMR for RIO-14;.

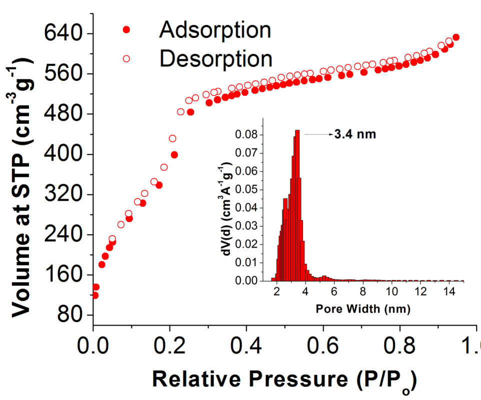

(a)

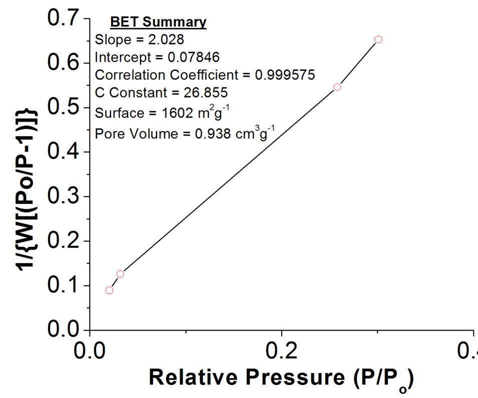

(b)

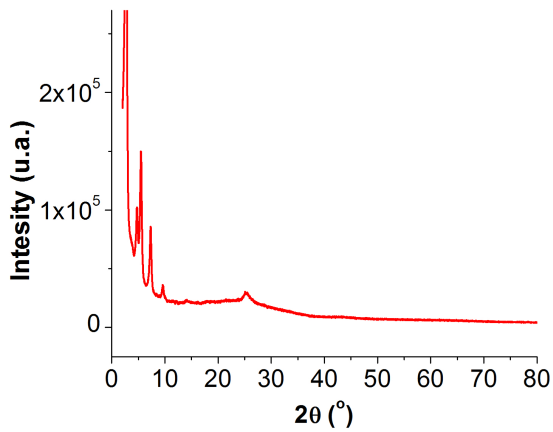

(c)

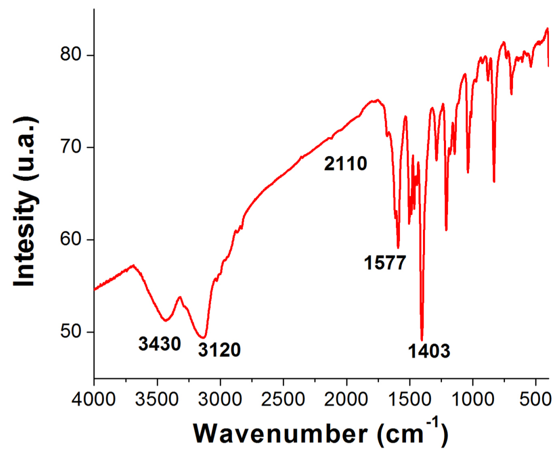

(d)

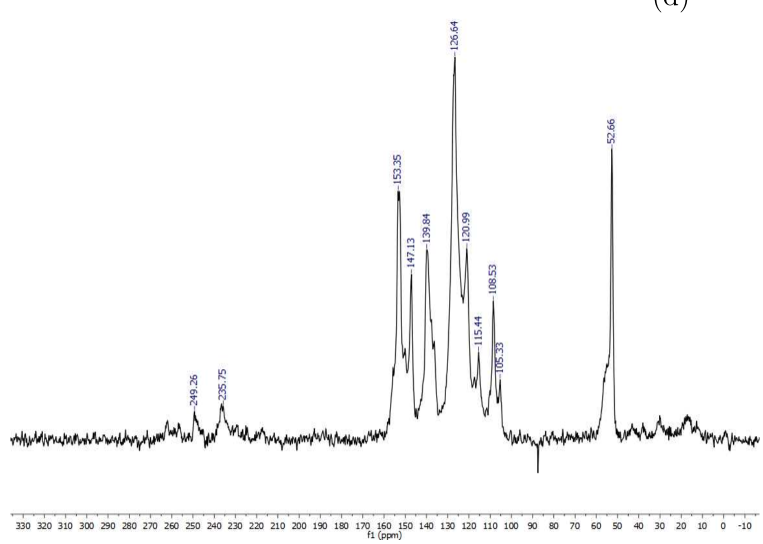

(e)

Figure S3: (a) Adsorption-desorption N_2 isotherm and pore size distribution using NLDFT equilibrium model for cylindrical pores. (b) Multi-point BET plot (c) PXRD, (d) FT-IR and (e) CP-MAS ^{13}C NMR for $[HC{\equiv}C]_{0.17}$TPB-DMTP-COF.

2.3 TPB-DMTP-COF SU4 and SU5

TPB-DMTP-COF SU4 and SU5 were prepared according to the literature,[7] employing a scale-up of 4 times and 5 times, regarding the pristine conditions of the limiting reagent 1,3,5-tri-(4-aminophenyl)benzene (0.08 mmol). The ^{13}C NMR of SU4 and SU5 were as reported in the literature, as an example, the ^{13}C NMR of SU4 is shown (Figure S4). The N_2 isotherms can be found in Figure S4 and Figure S5.

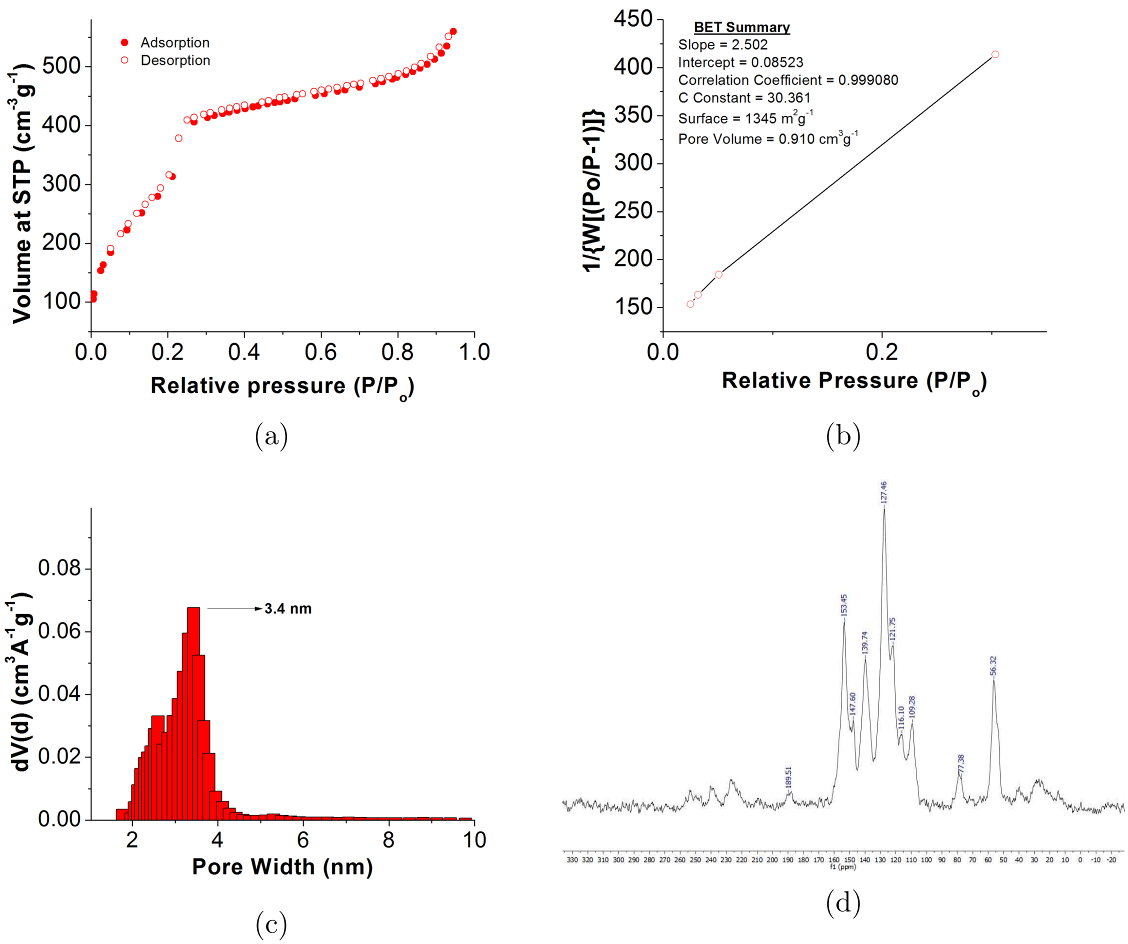

Figure S4: (a) Adsorption-desorption N_2 isotherm (b) Multi-point BET plot, (c) pore size distribution using NLDFT equilibrium model for cylindrical pores and (d) CP-MAS ^{13}C NMR for TPB-DMTP-COF SU4.

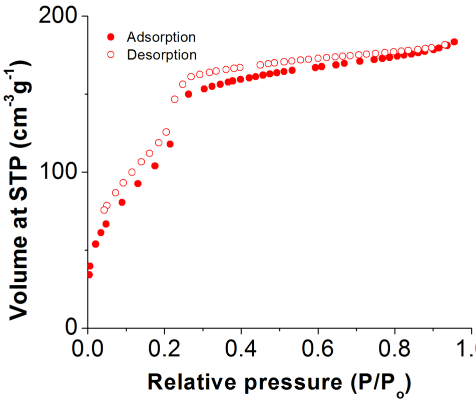

(a)

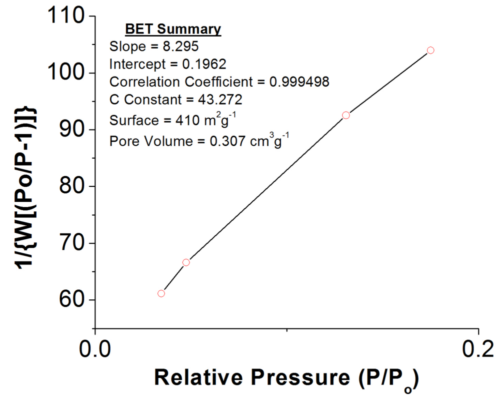

(b)

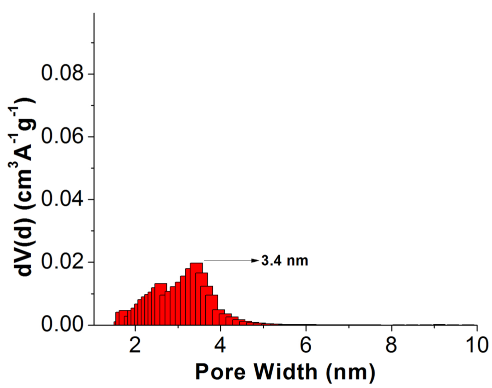

(c)

Figure S5: (a) Adsorption-desorption N_2 isotherm (b) Multi-point BET plot and (c) pore size distribution using NLDFT equilibrium model for cylindrical pores for TPB-DMTP-COF SU5.

3 Lattice Parameter for Mesoporous COFs

Table S1: Diffraction pattern (q values) for mesoporous COFs and lattice parameter (a) for hexagonal structures.

TPB-DMTP-COF	**Structure**	**Peak 1**	**Peak 2**	**Peak 3**	**Peak 4**	**Peak 5**	**Peak 6**	$\boldsymbol{a}$
Pristine	Hexagonal	2.0	3.4	4.0	5.3	6.9	17.9	3.6
SU4		2.0	3.4	4.0	5.3	6.9	17.9	3.6
SU5		1.9	3.4	4.0	5.3	6.9	18.8	3.8
$[HC{\equiv}C]_{0.17}$		2.0	3.4	4.0	5.3	6.9	17.9	3.6

4 Beaucage Modeling

Table S2: Beaucage parameters values for TPB-DMTP-COF SU5.

Parameters	Values
G	6.85257e+017
B	7.2e+006
G_s	2.5137e+007
B_s	1.3137e+007
R_g	≥ 60
R_{sub}	1.3
R_s	1.3
P	3.2
P_s	2

Table S3: Beaucage parameters values for $[HC{\equiv}C]_{0.17}$TPB-DMTP-COF.

Parameters	Values
G	7.19256e+015
B	3.17826e+006
G_s	1.01287e+007
B_s	1.37485e+007
R_g	≥ 55
R_{sub}	1.3
R_s	1.3
P	3.5
P_s	2.8

Table S4: Beaucage parameters values for $FeCl_3$@TPB-DMTP-COF 7.8%.

Parameters	Values
G	6.38572e+015
B	2.8e+006
G_s	6.87024e+006
B_s	6.25959e+006
R_g	≥ 54
R_{sub}	1.3
R_s	1.3
P	3.6
P_s	2.3

Table S5: Beaucage parameters values for $FeCl_3$@TPB-DMTP-COF 12%.

Parameters	Values
G	5e+006
B	2.6e+006
G_s	1.15563e+007
B_s	5.9e+006
R_g	$\geq$ 40
R_{sub}	1.3
R_s	1.3
P	3.9
P_s	1.9

5 WAXS Profile of Microporous COFs

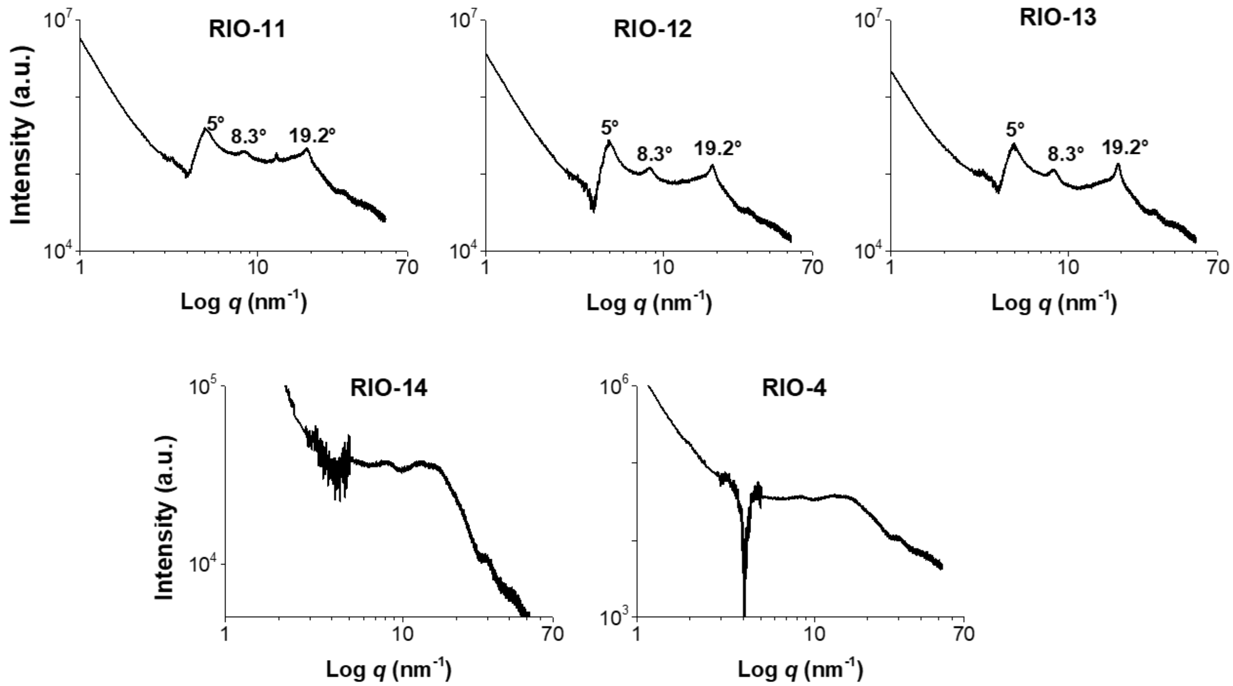

Figure S6: Diffraction profile for the microporous COFs for the WAXS range.

6 Scattering Techniques to Potentially Access Microporous COFs

Considering microporous COFs in general, it would be interesting to regularly combine SAXS with Wide-Angle X-ray Scattering (WAXS) and Ultra-Small-Angle X-Ray Scattering (USAXS) when analysing these types of materials. Since WAXS upper limit is around 30 nm^{-1}, this would allow the observation of even smaller features, granting a more in-depth view of the porous characteristics of these materials. Additionally, to obtain the radius of gyration by the Guinier's approximation for these specific microporous COFs, it would be necessary to access a lower-q region for the respective curves, which could be achieved by using USAXS. Thus, a combination of these three techniques (Figure S7) is suggested when one intends to thoroughly access the fractal characteristics of microporous materials employing the scattering data.

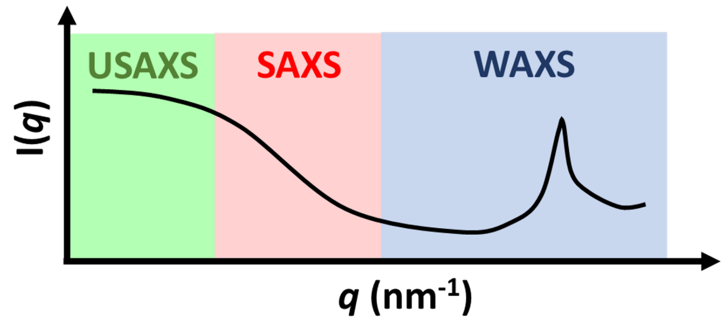

Figure S7: Schematic representation of the q range of the USAXS, SAXS and WAXS techniques.

References

(1) Guinier, A. La diffraction des rayons X aux très petits angles: application l'étude des phénomènes ultramicroscopiques. **1939**,

(2) Schnablegger, H.; Singh, Y. The SAXS guide: getting acquainted with the principles. *Austria: Anton Paar GmbH* **2011**, 1–124.

(3) Glatter, O.; Kratky, O. *Small angle X-ray scattering*; Academic press, 1982.

(4) Bale, H. D.; Schmidt, P. W. Small-angle X-ray-scattering investigation of submicroscopic porosity with fractal properties. *Physical Review Letters* **1984**, *53*, 596.

(5) Besselink, R.; Stawski, T.; Van Driessche, A.; Benning, L. G. Not just fractal surfaces, but surface fractal aggregates: Derivation of the expression for the structure factor and its applications. *The Journal of Chemical Physics* **2016**, *145*, 211908.

(6) Sinha, S.; Sirota, E.; Garoff,; S,; Stanley, H. X-ray and neutron scattering from rough surfaces. *Physical Review B* **1988**, *38*, 2297.

(7) Cifuentes, J. M.; Ferreira, B. X.; Esteves, P. M.; Buarque, C. D. Decarboxylative Cross-Coupling of Cinnamic Acids Catalyzed by Iron-Based Covalent Organic Frameworks. *Topics in Catalysis* **2018**, *61*, 689–698.